

# Observations and analysis of an urban boundary layer and sea breezes during extreme heat events

Gabriel Rios <sup>1\*</sup>, <sup>2\*</sup>, Prathap Ramamurthy <sup>1, 2</sup>

1. Department of Mechanical Engineering, CUNY City College, New York, New York
2. NOAA Center for Earth System Sciences and Remote Sensing Technologies, New York, New York

**Corresponding author:** Gabriel Rios ([grios001@citymail.cuny.edu](mailto:grios001@citymail.cuny.edu))

**\* Current affiliation(s):** Department of Mechanical Engineering, CUNY City College, New York, New York; NOAA Center for Earth System Sciences and Remote Sensing Technologies, New York, New York

For submission to the Quarterly Journal of the Royal Meteorological Society.

*Last updated:* February 15, 2022.

---

## **1 Abstract**

Extreme heat presents a significant risk to human health and infrastructure in cities. Several studies have been conducted in the past several decades to understand the interaction between the synoptic-scale extreme heat events and local-scale urban heat island effects. However, observations of boundary layer characteristics during these periods have been relatively rare. Our current understanding of urban boundary layer structure is incomplete, particularly in coastal environments where the local climatology is highly influenced by land-sea thermal gradients. In this study, we analyze the evolution and structure of the urban boundary layer during regular and extreme heat periods with the goal of better understanding the effect of extreme heat and sea breezes on the boundary layer over a coastal urban area. Our analysis focuses on the New York City metropolitan area and relies on observations from vertical profilers (Doppler lidar, microwave radiometer) and quantities derived by analytical methods. Additionally, satellite and reanalysis data are used to supplement observational data. Extreme heat events present a mean peak surface temperature increase of 7K, an increase of site-averaged specific humidity at the surface by 39.4%, and a marked southwesterly shift in winds at all sites. In addition, sea breeze events during heat extreme heat events are found to reduce temperatures and increase low-level moisture content from the early evening through nighttime hours, with strong variability between sites. The study also finds that extreme heat events unify horizontal wind directions throughout the boundary layer, and promote nocturnal onshore moisture transport.

## **19 1 Introduction**

Extreme heat poses a major risk to life and property. The effects of extreme heat are expected to impact cities especially, which presents a significant hazard for vulnerable populations and infrastructure. With regards to effects on public health, studies have shown that extreme and prolonged heat increases mortality and exacerbates existing health conditions in high-risk populations (Anderson and Bell, 2011; Frumkin, 2016; Heaviside, Macintyre, and Vardoulakis, 2017; Madrigano et al., 2015). With regards to effects on infrastructure, studies have shown that extreme heat subjects networks critical to urban areas (e.g., electrical grid, public transportation) under significant stresses and/or failure (McEvoy, Ahmed, and Mullett, 2012; Zuo et al., 2015). These events are projected to increase in frequency due to the effects of climate change. Projections indicate that the impacts of future climate will cause adverse effects of extreme heat to become more frequent and severe (Burillo et al., 2019; Forzieri et al., 2018; Peng et al., 2011).

31 The meteorology of extreme heat events and its impacts on urban areas can be observed from the synoptic  
32 and local scales. From a synoptic scale, extreme heat events are often caused by the sustained presence of  
33 a high-pressure system over an area, resulting in lower wind speeds and warm air subsidence, promoting  
34 higher surface temperatures (Black et al., 2004; Miralles et al., 2014). From a local perspective, the  
35 amplified impact of extreme heat events on cities is a result of the urban heat island (UHI) effect,  
36 which occurs as a result of the modification of land surface properties due to the built environment.  
37 The modification of surface properties has been shown to increase near-surface air temperatures due to  
38 factors such as radiation entrapment, increased heat storage, and lower evapotranspirative cooling (F.  
39 Chen, Yang, and Zhu, 2014; Dan Li and Elie Bou-Zeid, 2013; Ramamurthy and Bou-Zeid, 2017; Zhao  
40 et al., 2018). Additionally, urban areas near large bodies of water experience effects from the sea breeze,  
41 which has been shown to play a moderating influence on the intensity of the UHI effect (Hu and Xue,  
42 2016; Jiang et al., 2019; Stéfanon et al., 2014). The processes on these two scales can be connected by  
43 understanding the structure and dynamics of the urban boundary layer (UBL), which is the lowest part of  
44 the troposphere in which surface-atmosphere exchanges occur that directly affect human activity. There  
45 have been a large number of numerical studies performed to improve our understanding of UBL processes  
46 during extreme heat events, which have been important for conceptualizing the role of synoptic-scale  
47 and surface forcings on urban climate. Something about the vertical structure of the UBL and coupling  
48 these

49 However, detailed observational analyses of UBL structure and dynamics are somewhat limited, especially  
50 in the vertical direction. Over the last 20 years, microwave radiometers, lidars, and radiosondes have  
51 been shown to be essential for accomplishing this. Microwave radiometers have been used to determine  
52 vertical profiles of temperature and water vapor (Rose et al., 2005; Z. Wang et al., 2012), while lidars  
53 being used to observe three-dimensional wind fields and aerosol concentrations (Grund et al., 2001).  
54 Although radiosondes provide direct measurements of the aforementioned properties in the boundary  
55 layer as it moves vertically through it, they present greater difficulties (e.g., cost, shorter supply) and  
56 are unable to observe at the temporal resolution of microwave radiometers and lidars.

57 Although somewhat limited in spatiotemporal scale, numerous observational campaigns have been per-  
58 formed to better our understanding of UBL structure and dynamics. Barlow et al. (2011) provides an  
59 in-depth study of boundary layer dynamics above London over a month-long period using a combination  
60 of a sonic anemometer and Doppler lidar, allowing for high-resolution vertical observations of a complex  
61 UBL and a better understanding of turbulent structures and vertical mixing processes. Similarly, Pel-  
62 liccioni et al. (2012) employs a sonic anemometer and a sodar system at a site in Rome to observe and  
63 analyze the lower 200 m of the UBL to determine UBL characteristics and explore the validity of Monin-  
64 Obukhov similarity theory in the surface layer. Additionally, Arruda Moreira et al. (2020) evaluates the  
65 ability of lidar and microwave radiometer systems to observe turbulence over a variety of atmospheric  
66 conditions, including the effects of significant dust concentrations, in the region around Granada, Spain.  
67 Studies such as those performed by Banks et al. (2015), Quan et al. (2013), and Z. Wang et al. (2012)  
68 further demonstrate the ability of vertical profiling instruments to analyze the boundary layer structure  
69 by deriving UBL heights and its diurnal evolution. Expanding upon UBL structure, Anurose, Subra-  
70 hamanyam, and Sunilkumar (2018) details a long-term observational campaign over an urban location  
71 in southern India that chronicles UBL height through monsoon season, annual averages of near-surface  
72 quantities, and the dynamics and effects of the sea breeze circulation.

73 Observations of the UBL during extreme heat events are even more limited. Ramamurthy and Bou-Zeid  
74 (2017) used microwave radiometers to observe the UBL over New York City in July 2016 to find that  
75 the UHI effect was amplified during heat wave events and that spatial variability throughout the city  
76 was significant throughout the observation period. Jiang et al. (2019) explores the effects of heat waves  
77 on rural and urban areas for several cities in China using ground-based observations with a focus on the  
78 UHI effect, finding that the effect was amplified during heat waves due to greater surface solar radiation

79 and shifts in wind direction contributing to advection of heated air masses over the studied cities. (Wu  
80 et al., 2019) uses a combination of a ceilometer and multiple lidars to observe the evolution of UBL  
81 structure, air quality, and pollutant transport during a heat wave in New York City, demonstrating  
82 sharp rates of UBL growth due to convective activity and an increase of pollutant concentration and  
83 regional transport. Y. Zhang et al. (2020) uses aircraft-based observations to provide a comprehensive  
84 analysis of UBL structure during heat wave events over cities in the United States throughout a 10-year  
85 period, providing insights into the 'heat dome' thermodynamic structure over cities and the variability  
86 between heat wave events due to local (such as surface properties in urban areas) and large-scale (such  
87 as synoptic meteorological conditions) forcings.

88 New York City represents a complex case for urban meteorology given its diverse array of land cover  
89 types (deciduous forest to supertall skyscrapers) and its proximity to multiple major bodies of water  
90 (Lower New York Bay and the New York Bight to the south and east, Long Island Sound to the north  
91 and east). Due to these factors, the effects of the surface energy budget (Hrisko, Prathap Ramamurthy,  
92 and Gonzalez, 2021; Prathap Ramamurthy and Bou-Zeid, 2014; Tewari et al., 2019) and sea breezes  
93 (Childs and Raman, 2005; Colle and Novak, 2010; Frizzola and Fisher, 1963; Gedzelman et al., 2003;  
94 Melecio-Vázquez et al., 2018; Thompson, Holt, and Pullen, 2007) on the mesoscale meteorology have  
95 been studied extensively. However, similar to studies of other urban areas mentioned previously, much  
96 of this research has involved numerical simulations of these meteorological processes. In this study, we  
97 attempt to further our understanding of the UBL over a coastal urban area by compiling observations  
98 from multiple locations within New York City and analyzing the UBL using derived quantities.

99 This study attempts to use observations and analytical methods to provide insight into the following  
100 questions:

- 101 1. How do UBL structure and dynamics depart from the climatology during extreme heat events?
- 102 2. How do extreme heat events impact the transport of scalars?
- 103 3. What effect does the sea breeze have on a coastal urban area during extreme heat events?

## 104 2 Data collection and analysis

### 105 2.1 Study site

106 The UBL over New York City is observed and analyzed in this study. Observational data was captured  
107 at four locations within New York City (Table 1).

Table 1: Locations and details of observations sites.

	Bronx	Queens	Staten Island
Coordinates	40.87248°N, 73.89352°E	- 73.81585°E	- 74.14850°E
Elevation (m a.g.l.)	57.8	56.3	32.4
Element roughness height (m a.g.l.)			
Valid wind directions	N/A	180 to 360°	N/A

### 109 2.2 Observational instruments

110 Observations of the UBL were made using a synthesis of microwave radiometers, lidars, and satellites.

111  
112 Vertical profiles of temperature and vapor density were captured using a network of Radiometrics  
113 MP-3000A microwave radiometers (Hewison and Gaffard, 2003) operated by the New York State

114 Mesonet (Brotzge et al., 2020). Profiles for water vapor are retrieved using 21 channels in the 22-30.0  
115 GHz (K-band) range, while profiles for temperature are retrieved using 14 channels in the 51-59.0 GHz  
116 (V-band) range. Profile accuracy (relative to radiosonde soundings) determined by performance studies  
117 at various locations reported an annually-averaged water vapor accuracy within  $1.0 \text{ g m}^{-3}$  below 2 km  
118 and an annually-averaged temperature accuracy within 1.6 K below 4 km (Güldner and Spänkuch, 2001;  
119 Sánchez et al., 2013). Quantities are captured at 58 height levels starting at ground level and ending  
120 at 10 km above ground level, with vertical steps of 50 m from ground level to 500 m, 100 m from 500 m  
121 to 2 km, and 250 m steps above 2 km. Observation integration times range from 0.01 to 2.50 s. Vertical  
122 profiles are generated every 10 s and averaged over 10 min periods.

123

124 Wind measurements were measured using a network of Leosphere WindCube 100S Doppler lidars  
125 operated by the New York State Mesonet (Brotzge et al., 2020). Measurements of wind motion using  
126 the Doppler beam swinging scan mode in three directions: zonal ( $u$ ), meridional ( $v$ ), and vertical ( $w$ )  
127 over 20 s cycles, with measurements averaged over 10 min intervals (Shrestha et al., 2021). The vertical  
128 range of the WindCube 100S is 7 km above ground level with wind speed and direction accuracies of  
129  $0.5 \text{ m s}^{-1}$  and  $2^\circ$ , respectively. The WindCube 100S has also been shown to perform with a high degree  
130 of accuracy relative to radiosonde soundings, especially above 500 m (Kumer, Reuder, and Furevik, 2014).

131

132 Land and sea surface temperatures were estimated using derived products from the NOAA/NASA  
133 GOES-16 Advanced Baseline Imager (ABI) (Ignatov et al., 2010; Yu et al., 2008). The GOES-16 ABI  
134 provides a spatial resolution of 2 km with real-time data available to the public on an hourly basis.  
135 The spatial extent of the Land Surface Temperature (LST) product ranges from the continental United  
136 States (CONUS) to the majority of the Western Hemisphere (known as *full disk*), whereas the Sea  
137 Surface Temperature (SST) product has a full disk spatial extent. The LST product has been found  
138 to have an error relative to surface observations of 2.5 K over all land cover types, while sea surface  
139 temperatures (SSTs) estimated using the GOES-16 ABI have been found to have an error relative to  
140 shipborne radiometers  $\leq 1 \text{ K}$  in the New York Bight (Luo and Minnett, 2021).

#### 141 2.2.1 Data criteria & availability

142 Dates selected for this study are categorized into three groups: (1) normal days, (2) extreme heat days,  
143 and (3) sea breeze days. For the purposes of this study, *extreme heat events* are defined as 3 or more  
144 consecutive days with maximum daily temperatures exceeding 90°F (305 K), per the New York branch  
145 of NOAA National Weather Service (Robinson, 2001; National Weather Service, 2018), while *normal*  
146 *days* are defined as days that do not meet these criteria. Because the aim of this study is to observe the  
147 effect of extreme heat on the UBL, normal day selection was restricted to months in which extreme heat  
148 events occurred (May through September), as well as days in which 50% or more of the day featured  
149 clear-sky conditions below 3.65 km above ground level due to the association of extreme heat events with  
150 reduced daytime cloud coverage and precipitation (Stéfanon et al., 2014; Thomas et al., 2020). Clear-  
151 sky conditions were identified by using an average of 5-minute surface-based observations from three  
152 airports in the Automated Surface Observation System (ASOS) (NOAA et al., 1998) network within  
153 the New York City metropolitan area: Newark Liberty International Airport (EWR), John F. Kennedy  
154 International Airport, and LaGuardia Airport. *Sea breeze events* are identified as times during normal  
155 and extreme heat days in which the low-level ( $\leq 200 \text{ m}$ ) mean horizontal wind speed ( $U$ ) is less than  
156  $5 \text{ m s}^{-1}$  and low-level wind direction has a primarily easterly component, due to the presence of the  
157 Atlantic Ocean to the east of New York City.

158 - Discuss quality filtering - Plots showing sampling counts per hour per site per day

159 **2.3 Derived quantities**

160 **3 Normal and extreme heat boundary layer properties**

161 This section discusses the differences in boundary layer structure and properties between normal days  
162 and extreme heat events. Results are presented from the averages over all identified normal and heat  
163 event days.

164 **3.1 Temperature**

165 On average, extreme heat events increase the temperature at the surface, as expected (see Figure  
166 4). This is consistent across all observed locations in New York City, with the extreme heat event  
167 temperature exceeding normal temperatures by approximately  $1-\sigma$  over the entire day. An increase in  
168 the difference is observed during daytime hours, with the difference peaking in magnitude around 13:00  
169 LST at the hottest time of day. The surface temperature variability is significantly lower during heat  
170 events (average  $\sigma = 1.77\text{K}$ ) than during normal temperatures (average  $\sigma = 4.57\text{K}$ ). There is little  
171 spatial variability between sites, with maximum average temperatures ranging from 305.65 K in Queens  
172 to 306.63 K in the Bronx. It is worth noting that there are areas in New York City that are located  
173 in more heavily urbanized areas than the observation sites (such as Midtown Manhattan and central  
174 Brooklyn), so it is likely that certain areas within the city have higher maximum temperatures.

175  
176 Above the surface, extreme heat events increase the temperature significantly over the lowest  
177 3000 m of the troposphere (see Figure 3), with standardized anomalies of  $\theta$  ranging from  $\sigma = 0.99$  to  
178 1.30. The largest temperature anomalies shift from the surface layer in the mornings to span the entirety  
179 of the mixed layer. This is reflective of strong surface forcing resulting in convection through the mixed  
180 layer, as indicated by the formation of a late morning superadiabatic layer at all locations (Figures 5, 6, 7).

181  
182 These vertical profiles of  $\theta$  suggest a degree of spatial variability in the UBL exists between loca-  
183 tions. One instance of this spatial variability is vertical mixing; the Bronx site appears to have  
184 stronger vertical mixing as shown in Figure 5, as  $\theta$  remains constant for a greater height than at  
185 the Queens and Staten Island locations, indicating a deeper mixed layer. This phenomenon is more  
186 pronounced during extreme heat events, as a distinct mixed layer is apparent in the Bronx during early  
187 (12:00 LST) and late (18:00 LST) afternoon hours. While a deepened mixed layer during extreme heat  
188 events is also visible for the other locations, the strength of vertical mixing in the Bronx is emphasized  
189 by persistent afternoon instability as shown by negative  $\frac{d\theta}{dz}$  values between 500 and 1000 m and a  
190 superadiabatic surface layer and 12:00 and 18:00 LST.

191 **3.2 Moisture**

192 On average, extreme heat events were found to increase the moisture at the surface, as indicated by  
193 the diurnal profiles of specific humidity ( $q$ ) (see Figure 9). This is also consistent across all observed  
194 locations in New York City, with the extreme heat event temperature exceeding normal temperatures  
195 by approximately  $1-\sigma$  over the entire day. Although a distinct diurnal profiles exists ( $q$  decreases during  
196 daytime hours), the diurnal range is smaller in magnitude than temperature. It is also worth noting  
197 that the diurnal range is lower for Staten Island than for the Bronx or Queens, suggesting that degree of  
198 urbanization has a negative correlation with the diurnal range of  $q$ . Similar to surface temperature, the  
199 variability of  $q$  is significantly lower during heat events (average  $\sigma = 2.14 \times 10^{-3} \text{ kg kg}^{-1}$ ) than during  
200 normal temperatures (average  $\sigma = 3.18 \times 10^{-3} \text{ kg kg}^{-1}$ ). Queens shows exceptional variability in  $q$ ,  
201 which may be attributed to the location of the observation site, which is adjacent to Flushing Meadows  
202 Corona Park (large open vegetated space), is surrounded by a medium-density urban area on all other  
203 sides, and is approximately 4 km from Long Island Sound.

204

205 In the boundary layer, the positive  $q$  anomalies subside in magnitude between 300 and 600 m,  
 206 but increase significantly in the mixed layer, especially during the late morning and early afternoon for  
 207 all sites. As shown in Figure 8, the largest anomalies occur between 10:00 and 16:00 LST throughout the  
 208 mixed layer. With regards to spatial variation in  $q$ , Staten Island demonstrates a strong positive anomaly  
 209 overnight through the early morning near the surface, indicating elevated low-level moisture transport  
 210 during extreme heat events, whereas the Bronx and Queens demonstrate a similar phenomenon with  
 211 a lesser anomaly magnitude. All sites show significant positive  $q$  anomalies throughout the day, with  
 212 the strongest anomaly signal starting in the low-levels throughout the morning and transitioning to the  
 213 mixed later by mid-afternoon. This trend suggests that the increase in nocturnal low-level moisture  
 214 corresponds to increased UBL moisture content due to strong vertical mixing throughout the daytime.

215

216 This is supported by Figures 10, 11, 12, where vertical profiles of  $q$  across all locations show  
 217 markedly higher  $q$  values at the surface during extreme heat events with  $\frac{dq}{dz}$  values increasing throughout  
 218 the morning in the mixed layer while low-level  $q$  values decrease, indicating vertical transport of moisture  
 219 and drier low-level conditions during peak insolation. The strong vertical mixing of  $q$  can be observed  
 220 at all sites, where late morning and early afternoon  $\frac{dq}{dz}$  values are greater during extreme heat events  
 221 than normal days. An example can be seen in the Bronx, where  $\frac{dq}{dz} > 0$ , indicating very efficient vertical  
 222 moisture transport.

### 223 3.3 UBL dynamics

#### 224 3.3.1 Horizontal winds

225 Extreme heat events coincided with an overall reduction of horizontal wind speeds ( $U$ ) in the UBL  
 226 (Figure 13). More specifically, the magnitude of  $U$  during extreme heat events is similar in magnitude  
 227 to  $U$  during normal days with the exception of early morning hours and at upper levels of the UBL. As  
 228 shown in Figure 14, modest reductions in  $U$  ( $-1.2 \leq \sigma \leq -0.4$ ) during extreme heat events are present  
 229 throughout the UBL from early to mid-morning, with little difference throughout the rest of the day  
 230 ( $-0.4 \leq \sigma \leq 0.4$ ). Larger deviations between  $U$  values are present at the top of the UBL where synoptic  
 231 conditions become dominant.

232

233 Vertical profiles of  $U$  for normal and extreme heat events provide a more detailed view of the  
 234 differences in UBL structure. Across all sites,  $U$  is similar throughout the UBL overnight, afternoon,  
 235 and evenings. During early morning hours, however, extreme heat event  $U$  values decrease by 25  
 236 to 50% throughout the entire UBL (see Figures 15, 16, 17), although both event types present a  
 237 classical logarithmic wind profile, with surface friction effects present through 500 m. The reduction  
 238 in  $U$  during extreme heat events is likely due to the presence of an anticyclonic circulation that  
 239 suppresses the nocturnal low-level jet over New York City (T. C. Chen and Kpaeyeh, 1993). Another  
 240 phenomenon worth noting is the difference in  $U$  profiles above 2000 m; profiles of  $U$  during extreme  
 241 heat events are more consistent between sites and vertically than during normal days. This phe-  
 242 nomenon is the effect of synoptic meteorological conditions on  $U$ , as the UBL typically remains below  
 243 2500 m. During extreme heat events, anticyclonic conditions produce more consistent atmospheric con-  
 244 ditions relative to normal days, resulting in less variability between heat events than during normal days.

245

246 Extreme heat events result in a southwesterly shift in  $U$  throughout the UBL. This shift is present most  
 247 evidently closer to the surface, as shown in Figures 18, 19, and 20, with winds at 100 m coming primarily  
 248 from the southwest quadrant. Figure 19 shows that Queens also presents a secondary maximum with  
 249 winds approaching from the south, which suggests effects from the Atlantic sea breeze (effects from  
 250 the sea breeze will be further discussed in Section 4). At 1000 m, the directionality of prevailing winds  
 251 becomes more uniform between normal and extreme heat days, as winds primarily approach New York

252 City from the west-southwest. The disparity in wind directions between 100 and 1000 m suggests that  
253 localized wind fields play a more significant role in UBL dynamics at lower levels whereas synoptic-scale  
254 atmospheric conditions increasingly dominate with increasing height. Regardless, the uniformity of  
255 wind direction during extreme heat relative to normal days indicates that synoptic-scale effects can  
256 play a larger role at lower levels due to advection from the continent, especially with regards to thermal  
257 advection that leads to the transport of heated inland air masses over New York City (Ramamurthy, Li,  
258 and Bou-Zeid, 2017).

### 259 3.3.2 Vertical motion

260 On average, extreme heat events do not appear to produce significant changes in vertical velocity ( $w$ ).  
261 Figure 21 shows average diurnal profiles of  $w$  at all locations at 100 m above ground level, with similar  
262 mean values throughout the day between normal days and extreme heat events. During extreme heat  
263 events, however, the variability of  $w$  is less in the early morning hours and greater in the evening. This  
264 phenomenon is also observed in vertical profiles of  $w$  at all locations as shown in Figures 23, 24, and  
265 25. At all locations, overnight and morning profiles of  $w$  (0:00 and 6:00 LST) show significantly lower  
266 variability in  $w$  throughout the UBL with similar magnitudes of mean  $w$ . Despite similar means and  
267 deviations in the early afternoon (12:00 LST), evening profiles (18:00 LST) show significantly higher  
268 variability in  $w$  below 500 m for all sites, with the Bronx showing this occurrence extend through the  
269 UBL. The similarity in vertical profiles of  $w$  may be a result of a balance between large-scale subsidence  
270 (due to the presence of high-pressure during extreme heat events) and the effects of increased surface  
271 forcings during extreme heat events relative to normal days (Dong et al., 2018; D.-L. Zhang, Shou, and  
272 Dickerson, 2009).

## 273 4 Effects of the sea breeze circulation

274 Sea breezes in New York City occur as a result of land-sea temperature gradients from two arms of the  
275 Atlantic Ocean; the New York Bight to the southeast and Long Island Sound to the northeast. Sea  
276 breezes from both bodies increase the complexity of UBL dynamics over New York City due to the  
277 coalescence of opposing fronts over a complex topography (Bornstein and Thompson, 1981). A typical  
278 sea breeze event in New York City is defined by calm ambient low-level winds ( $\leq 5 \text{ m s}^{-1}$ , the formation  
279 of a large land-sea temperature gradient in the mid- to late morning, strong late-morning thermals  
280 that promote low-level convergence, and afternoon to early-evening onshore moisture transport and  
281 reduction in surface air temperatures (especially in areas closest to the shore) (Childs and Raman, 2005;  
282 Frizzola and Fisher, 1963; Gedzelman et al., 2003).

283  
284 Sea breeze events occurred on approximately 56% of all days observed. The high frequency of  
285 occurrence is attributable to low-level convergence due to the large land-sea temperature gradient that  
286 is common during warmer months (Childs and Raman, 2005; Gedzelman et al., 2003; Thompson, Holt,  
287 and Pullen, 2007), as days were chosen exclusively between May and September. Maximum land-sea  
288 surface temperature differences during days with identifiable sea breeze events averaged at 12 K, with a  
289 strong diurnal profile with the peak difference occurring around midday (see Figure 26). The frequency  
290 of occurrence increases when observing days during extreme heat events, as the lack of a strong synoptic  
291 wind allows for the sea breeze circulation to become dominant in the metropolitan area (Miller et al.,  
292 2003).

### 293 4.1 UBL structure during sea breeze events

294 During normal days, observations show that the sea breeze reduces temperature and increases moisture  
295 content throughout the UBL after 12:00 LST. In Figure 27, the standardized anomalies of  $\theta$  between  
296 normal days with and without a sea breeze are shown, averaged over all days on an hourly basis.

297 Overnight and in the early morning, positive anomalies of  $\theta$  are present above the UBL ( $\leq 1\text{ km}$ )  
298 until mid-morning, with the Bronx having the most significant anomaly and Staten Island the least.  
299 This suggests a decreasing degree of anomalous  $\theta$  with decreasing urbanization. This anomaly pattern  
300 coincides with a positive  $q$  anomaly trend in both the spatiotemporal aspect (peak anomaly occurs above  
301 1 km before 8:00 LST) and the magnitude aspect (the Bronx has the most significant early morning  
302 anomaly, Staten Island has the least). Later in the day, all sites observe a negative  $\theta$  anomaly throughout  
303 the UBL despite a negative  $q$  anomaly, indicating that sea breeze events during normal days coincide  
304 with a cooler and drier daytime UBL before the onset of the sea breeze. Sea breeze effects become  
305 apparent during the mid-afternoon with the presence of a significant negative  $\theta$  and positive  $q$  anomaly  
306 in the lower UBL, with Staten Island experiencing effects first (approximately 16:00 LST) and the Bronx  
307 experiencing effects last (approximately 19:00 LST). It is worth noting that the  $q$  anomaly is weak-  
308 est in the Bronx, which suggests that the sea breeze front weakens as it travels inland over New York City.  
309

310 During extreme heat events, observations show that the sea breeze plays a moderating role on  
311 surface conditions by reducing low-level temperatures and increasing low-level moisture content, similar  
312 to phenomena observed during normal days. In Figure 29, the standardized anomalies of  $\theta$  between  
313 extreme heat days with and without a sea breeze are shown, averaged over all days. All sites shown  
314 that extreme heat days with a sea breeze possess slightly higher values of  $\theta$  in the mid-morning,  
315 with significant low-level reduction in  $\theta$  in the afternoon and evening. On average, the onset of the  
316 low-level cooling occurs in Staten Island first at approximately 12:00 LST, with Queens following at  
317 approximately 14:00 LST, and the Bronx at about 18:00 LST. This disparity in times appears to  
318 represent the passage of the southeasterly sea breeze front through New York City, where the onset  
319 time correlates with the distance from the New York Bight (Bornstein and Thompson, 1981). A similar  
320 phenomenon is observed by the transport of  $q$  as shown in Figure 30, with drier conditions throughout  
321 the UBL before 12:00 LST and increasing low-level moisture as the day progresses. With regards to  
322 onset,  $q$  follows a similar pattern to  $\theta$  in that the onset time is dependent from distance to the shore.  
323 These anomalies present most significantly in the lowest 1000 m of the UBL after 12:00 LST, which  
324 aligns with sea breeze circulation characteristics observed in Frizzola and Fisher (1963).

## 325 4.2 UBL dynamics during sea breeze events

326 Days with identifiable sea breeze events had lower  $U$  throughout the majority of the UBL, with the  
327 most significant decreases during the nighttime, potentially due to the lessening of onshore flow due  
328 to the reduction of the land-sea temperature gradient (Pullen et al., 2007), as shown in Figure 26.  
329 Vertical motions, however, increased significantly in the Bronx and Queens during the late morning and  
330 early afternoon, as shown in Figure 31. These anomalies indicate the increased presence of updrafts in  
331 urbanized areas which contribute to low-level convergence, promoting onshore flow in the afternoon and  
332 evening.

333

334 During extreme heat days with identified sea breeze circulations, easterly winds increase in fre-  
335 quency in the lower levels of the UBL, as shown in Figures 32, 33, and 34. These winds are the result  
336 of onshore flow from the New York Bight (southeasterly) and Long Island Sound (northeasterly).

337 During extreme heat days with sea breeze circulations, southeasterly winds increased in frequency com-  
338 pared to all other directions at all locations. The occurrence frequency of southeasterly winds is correlated  
339 with the distance between the observation site and the largest body of water in proximity of the metropoli-  
340 tan area (Atlantic Ocean), as Staten Island reported 92.1% of all winds at 100 m as southeasterly between  
341 12:00 and 20:00 LST (distance of 6.50 km from Lower New York Bay), whereas Queens reported 67.4%  
342 (distance of 16.5 km) and Bronx reported 55.6% (distance of 32.9 km) during the same time interval.  
343 The disparity in southeasterly winds further demonstrates the spatial extent and progression of the sea  
344 breeze front.

345 For sites near Long Island Sound (the Bronx and Queens), northeasterly winds increased in frequency

as well, though not to the same magnitude as southeasterly winds. This disparity in magnitude suggests that the Long Island Sound sea breeze front is weaker than the New York Bight sea breeze front, which aligns with previous studies of sea breeze fronts over New York City (Frizzola and Fisher, 1963; Meir et al., 2013). Northeasterly winds increased in frequency during extreme heat days with sea breeze circulations, with a notable increase in the early morning hours (a likely result of nocturnal low-level motion) and in the evening hours (signal of a Long Island Sound sea breeze). This phenomenon is also apparent in Queens and Staten Island, albeit to a lesser frequency.

## 5 Conclusions

- How do UBL structure and dynamics depart from the climatology during extreme heat events?
- How does the UBL structure impact the transport of scalars?
- The sea breeze reduces temperatures throughout the UBL after the onset of the sea breeze, which typically occurs in the mid-afternoon in immediate coastal areas and in the evening for areas further inland. The sea breeze also results in nocturnal low-level onshore moisture transport.

## Acknowledgments

This research is made possible by the New York State (NYS) Mesonet. Original funding for the NYS Mesonet was provided by Federal Emergency Management Agency grant FEMA-4085-DR-NY, with the continued support of the NYS Division of Homeland Security & Emergency Services; the state of New York; the Research Foundation for the State University of New York (SUNY); the University at Albany, SUNY; the Atmospheric Sciences Research Center (ASRC) at SUNY Albany; and the Department of Atmospheric and Environmental Sciences (DAES) at SUNY Albany.

## References

- Anderson, G Brooke and Michelle L Bell (2011). “Heat waves in the United States: mortality risk during heat waves and effect modification by heat wave characteristics in 43 US communities”. In: *Environmental health perspectives* 119.2, pp. 210–218.
- Anurose, TJ, D Bala Subrahmanyam, and SV Sunilkumar (2018). “Two years observations on the diurnal evolution of coastal atmospheric boundary layer features over Thiruvananthapuram (8.5° N, 76.9° E), India”. In: *Theoretical and applied climatology* 131.1, pp. 77–90.
- Arruda Moreira, Gregori de et al. (2020). “Study of the planetary boundary layer height in an urban environment using a combination of microwave radiometer and ceilometer”. In: *Atmospheric Research* 240, p. 104932.
- Banks, Robert F et al. (2015). “Performance evaluation of the boundary-layer height from lidar and the Weather Research and Forecasting model at an urban coastal site in the north-east Iberian Peninsula”. In: *Boundary-layer meteorology* 157.2, pp. 265–292.
- Barlow, Janet F et al. (2011). “Boundary layer dynamics over London, UK, as observed using Doppler lidar during REPARTEE-II”. In: *Atmospheric Chemistry and Physics* 11.5, pp. 2111–2125.
- Black, Emily et al. (2004). “Factors contributing to the summer 2003 European heatwave”. In: *Weather* 59.8, pp. 217–223.
- Bornstein, Robert D and William T Thompson (1981). “Effects of frictionally retarded sea breeze and synoptic frontal passages on sulfur dioxide concentrations in New York City”. In: *Journal of Applied Meteorology and Climatology* 20.8, pp. 843–858.
- Brotzge, Jerald A et al. (2020). “A technical overview of the new york state mesonet standard network”. In: *Journal of Atmospheric and Oceanic Technology* 37.10, pp. 1827–1845.
- Burillo, Daniel et al. (2019). “Electricity infrastructure vulnerabilities due to long-term growth and extreme heat from climate change in Los Angeles County”. In: *Energy Policy* 128, pp. 943–953.

- 389 Chen, Feng, Xuchao Yang, and Weiping Zhu (2014). "WRF simulations of urban heat island under hot-weather  
390 synoptic conditions: The case study of Hangzhou City, China". In: *Atmospheric research* 138, pp. 364–377.
- 391 Chen, T C and J Alvin Kpaeyeh (1993). "The synoptic-scale environment associated with the low-level jet of the  
392 Great Plains". In: *Monthly weather review* 121.2, pp. 416–420.
- 393 Childs, Peter P and Sethu Raman (2005). "Observations and numerical simulations of urban heat island and sea  
394 breeze circulations over New York City". In: *Pure and Applied Geophysics* 162.10, pp. 1955–1980.
- 395 Colle, Brian A and David R Novak (2010). "The New York Bight jet: climatology and dynamical evolution". In:  
396 *Monthly Weather Review* 138.6, pp. 2385–2404.
- 397 Dong, Li et al. (2018). "The dynamical linkage of atmospheric blocking to drought, heatwave and urban heat  
398 island in southeastern US: A multi-scale case study". In: *Atmosphere* 9.1, p. 33.
- 399 Forzieri, Giovanni et al. (2018). "Escalating impacts of climate extremes on critical infrastructures in Europe".  
400 In: *Global environmental change* 48, pp. 97–107.
- 401 Frizzola, John A and Edwin L Fisher (1963). "A series of sea breeze observations in the New York City area".  
402 In: *Journal of Applied Meteorology and Climatology* 2.6, pp. 722–739.
- 403 Frumkin, Howard (2016). "Urban sprawl and public health". In: *Public health reports*.
- 404 Gedzelman, SD et al. (2003). "Mesoscale aspects of the urban heat island around New York City". In: *Theoretical  
405 and applied climatology* 75.1, pp. 29–42.
- 406 Grund, Christian J et al. (2001). "High-resolution Doppler lidar for boundary layer and cloud research". In:  
407 *Journal of Atmospheric and Oceanic Technology* 18.3, pp. 376–393.
- 408 Guldner, J and D Späckkuch (2001). "Remote sensing of the thermodynamic state of the atmospheric boundary  
409 layer by ground-based microwave radiometry". In: *Journal of Atmospheric and Oceanic Technology* 18.6,  
410 pp. 925–933.
- 411 Heaviside, Clare, Helen Macintyre, and Sotiris Vardoulakis (2017). "The urban heat island: implications for health  
412 in a changing environment". In: *Current environmental health reports* 4.3, pp. 296–305.
- 413 Hewison, Tim and Catherine Gaffard (2003). "Radiometrics MP3000 microwave radiometer performance assess-  
414 ment". In: *Obs. Development Technical Report TR29, Met Office, National Meteorological Library, Exeter,  
415 UK. Also available from <http://tim.hewison.org/TR29.pdf>*.
- 416 Hrisko, Joshua, Prathap Ramamurthy, and Jorge E Gonzalez (2021). "Estimating heat storage in urban areas  
417 using multispectral satellite data and machine learning". In: *Remote Sensing of Environment* 252, p. 112125.
- 418 Hu, Xiao-Ming and Ming Xue (2016). "Influence of synoptic sea-breeze fronts on the urban heat island intensity  
419 in Dallas–Fort Worth, Texas". In: *Monthly Weather Review* 144.4, pp. 1487–1507.
- 420 Ignatov, A et al. (2010). "GOES-R Advanced Baseline Imager (ABI) algorithm theoretical basis document for  
421 sea surface temperature". In: *NOAA NESDIS Center for Satellite Applications and Research*.
- 422 Jiang, Shaojing et al. (2019). "Amplified urban heat islands during heat wave periods". In: *Journal of Geophysical  
423 Research: Atmospheres* 124.14, pp. 7797–7812.
- 424 Kumer, Valerie-M, Joachim Reuder, and Birgitte R Furevik (2014). "A comparison of LiDAR and radiosonde  
425 wind measurements". In: *Energy Procedia* 53, pp. 214–220.
- 426 Li, Dan and Elie Bou-Zeid (2013). "Synergistic interactions between urban heat islands and heat waves: The  
427 impact in cities is larger than the sum of its parts". In: *Journal of Applied Meteorology and Climatology* 52.9,  
428 pp. 2051–2064.
- 429 Luo, Bingkun and Peter J Minnett (2021). "Skin Sea Surface Temperatures From the GOES-16 ABI Validated  
430 With Those of the Shipborne M-AERI". In: *IEEE Transactions on Geoscience and Remote Sensing* 59.12,  
431 pp. 9902–9913.
- 432 Madrigano, Jaime et al. (2015). "A case-only study of vulnerability to heat wave-related mortality in New York  
433 City (2000–2011)". In: *Environmental health perspectives* 123.7, pp. 672–678.
- 434 McEvoy, Darryn, Iftekhar Ahmed, and Jane Mullett (2012). "The impact of the 2009 heat wave on Melbourne's  
435 critical infrastructure". In: *Local Environment* 17.8, pp. 783–796.
- 436 Meir, Talmor et al. (2013). "Forecasting the New York City urban heat island and sea breeze during extreme  
437 heat events". In: *Weather and Forecasting* 28.6, pp. 1460–1477.
- 438 Melecio-Vázquez, David et al. (2018). "Thermal Structure of a Coastal–Urban Boundary Layer". In: *Boundary-  
439 Layer Meteorology* 169 (1), pp. 151–161. ISSN: 15731472.
- 440 Miller, STK et al. (2003). "Sea breeze: Structure, forecasting, and impacts". In: *Reviews of geophysics* 41.3.
- 441 Miralles, Diego G et al. (2014). "Mega-heatwave temperatures due to combined soil desiccation and atmospheric  
442 heat accumulation". In: *Nature geoscience* 7.5, pp. 345–349.

- 443 National Weather Service, NOAA (May 2018). *National Weather Service New York, NY excessive heat page*. URL:  
444 <https://www.weather.gov/okx/excessiveheat>.
- 445 NOAA et al. (1998). *Automated Surface Observing System (ASOS) User's Guide*. URL: <https://www.weather.gov/media/asos/aum-toc.pdf>.
- 447 Pelliccioni, A et al. (2012). "Some characteristics of the urban boundary layer above Rome, Italy, and applicability  
448 of Monin–Obukhov similarity". In: *Environmental fluid mechanics* 12.5, pp. 405–428.
- 449 Peng, Roger D et al. (2011). "Toward a quantitative estimate of future heat wave mortality under global climate  
450 change". In: *Environmental health perspectives* 119.5, pp. 701–706.
- 451 Pullen, Julie et al. (2007). "Atmospheric response to local upwelling in the vicinity of New York–New Jersey  
452 harbor". In: *Journal of applied meteorology and climatology* 46.7, pp. 1031–1052.
- 453 Quan, Jiannong et al. (2013). "Evolution of planetary boundary layer under different weather conditions, and its  
454 impact on aerosol concentrations". In: *Particuology* 11.1, pp. 34–40.
- 455 Ramamurthy, P and E Bou-Zeid (2017). "Heatwaves and urban heat islands: a comparative analysis of multiple  
456 cities". In: *Journal of Geophysical Research: Atmospheres* 122.1, pp. 168–178.
- 457 Ramamurthy, P, D Li, and E Bou-Zeid (2017). "High-resolution simulation of heatwave events in New York  
458 City". In: *Theoretical and applied climatology* 128.1, pp. 89–102.
- 459 Ramamurthy, Prathap and E Bou-Zeid (2014). "Contribution of impervious surfaces to urban evaporation". In:  
460 *Water Resources Research* 50.4, pp. 2889–2902.
- 461 Robinson, Peter J (2001). "On the definition of a heat wave". In: *Journal of Applied Meteorology and Climatology*  
462 40.4, pp. 762–775.
- 463 Rose, Thomas et al. (2005). "A network suitable microwave radiometer for operational monitoring of the cloudy  
464 atmosphere". In: *Atmospheric research* 75.3, pp. 183–200.
- 465 Sánchez, JL et al. (2013). "A method to improve the accuracy of continuous measuring of vertical profiles of  
466 temperature and water vapor density by means of a ground-based microwave radiometer". In: *Atmospheric  
467 Research* 122, pp. 43–54.
- 468 Shrestha, Bhupal et al. (2021). "Overview and Applications of the New York State Mesonet Profiler Network".  
469 In: *Journal of Applied Meteorology and Climatology* 60.11, pp. 1591–1611.
- 470 Stéfanon, Marc et al. (2014). "Soil moisture-temperature feedbacks at meso-scale during summer heat waves over  
471 Western Europe". In: *Climate dynamics* 42.5, pp. 1309–1324.
- 472 Tewari, Mukul et al. (2019). "Interaction of urban heat islands and heat waves under current and future climate  
473 conditions and their mitigation using green and cool roofs in New York City and Phoenix, Arizona". In:  
474 *Environmental Research Letters* 14.3, p. 034002.
- 475 Thomas, Natalie P et al. (2020). "Mechanisms associated with daytime and nighttime heat waves over the  
476 contiguous united states". In: *Journal of Applied Meteorology and Climatology* 59.11, pp. 1865–1882.
- 477 Thompson, William T, Teddy Holt, and Julie Pullen (2007). "Investigation of a sea breeze front in an urban envi-  
478 ronment". In: *Quarterly Journal of the Royal Meteorological Society: A journal of the atmospheric sciences,  
479 applied meteorology and physical oceanography* 133.624, pp. 579–594.
- 480 Wang, Z et al. (2012). "Lidar measurement of planetary boundary layer height and comparison with microwave  
481 profiling radiometer observation". In: *Atmospheric Measurement Techniques* 5.8, pp. 1965–1972.
- 482 Wu, Yonghua et al. (2019). "Observation of heat wave effects on the urban air quality and PBL in New York  
483 City area". In: *Atmospheric Environment* 218, p. 117024.
- 484 Yu, Yunyue et al. (2008). "Developing algorithm for operational GOES-R land surface temperature product". In:  
485 *IEEE Transactions on Geoscience and Remote Sensing* 47.3, pp. 936–951.
- 486 Zhang, Da-Lin, Yi-Xuan Shou, and Russell R Dickerson (2009). "Upstream urbanization exacerbates urban heat  
487 island effects". In: *Geophysical Research Letters* 36.24.
- 488 Zhang, Yuanjie et al. (2020). "Aircraft observed diurnal variations of the planetary boundary layer under heat  
489 waves". In: *Atmospheric Research* 235, p. 104801.
- 490 Zhao, Lei et al. (2018). "Interactions between urban heat islands and heat waves". In: *Environmental research  
491 letters* 13.3, p. 034003.
- 492 Zuo, Jian et al. (2015). "Impacts of heat waves and corresponding measures: a review". In: *Journal of Cleaner  
493 Production* 92, pp. 1–12.

<sup>494</sup> **Appendix**

$$p = p_0 \exp \frac{-gz}{RT_0}$$

$$\theta = T \left( \frac{p_0}{p} \right)^{\frac{R}{c_p}}$$

$$q = \frac{w}{1+w} = \frac{\frac{\varepsilon \rho'_v R_v T}{p - \rho'_v R_v T}}{1 + \frac{\varepsilon \rho'_v R_v T}{p - \rho'_v R_v T}}$$

$$Ri_b = \frac{g \Delta \bar{\theta}_v \Delta z}{\bar{\theta}_v [(\Delta \bar{U}^2) + (\Delta \bar{V}^2)]}$$

Table 2: Symbols and abbreviations used in the paper.

Symbol/Abbreviation	Definition
$\sigma$	Standard deviation
$\theta$	Potential temperature
$q$	Specific humidity
$U$	Horizontal wind speed
$w$	Vertical velocity
UBL	Urban boundary layer
MLH	Mixed layer height

<sup>495</sup>

<sup>496</sup> **Figures**

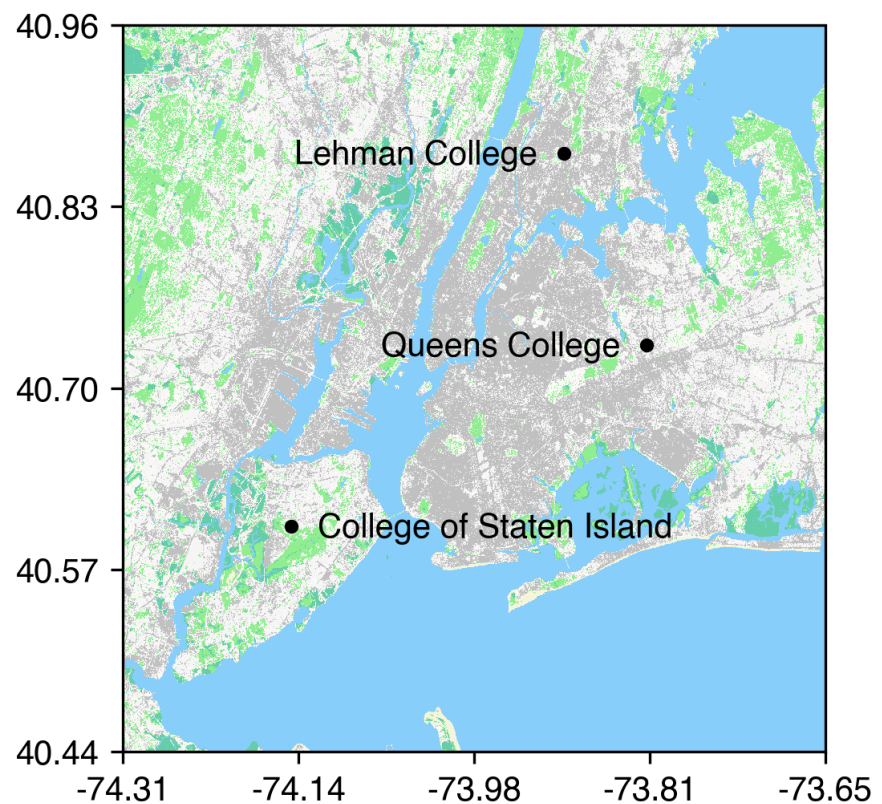


Figure 1: Observation sites overlaid on NLCD land cover types..

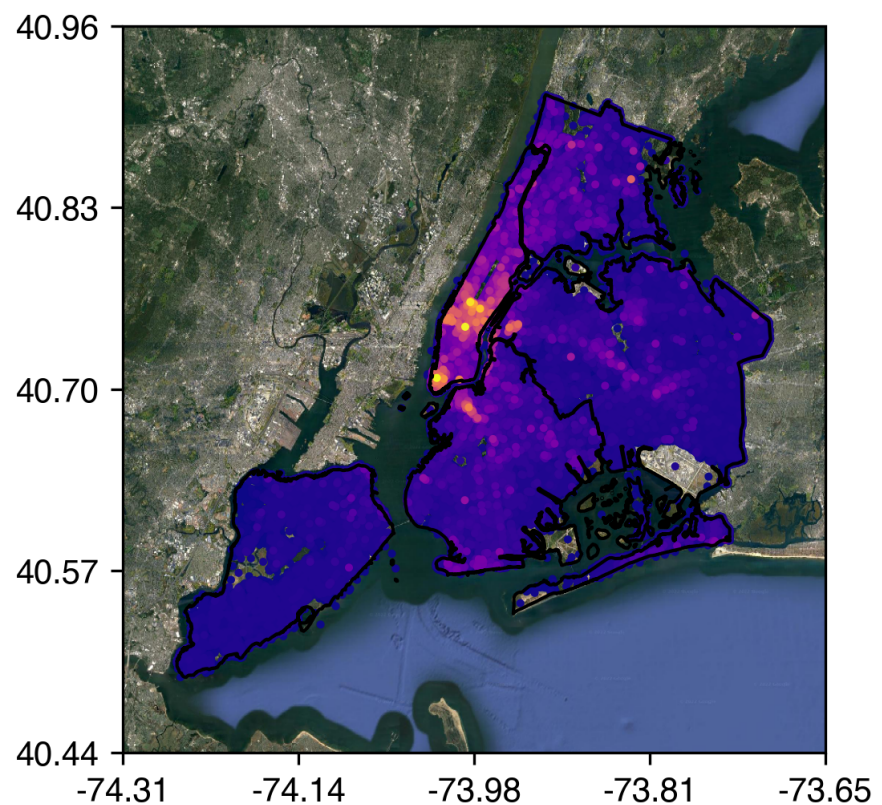


Figure 2: Building heights in New York City. Taken from NYC DOB data.

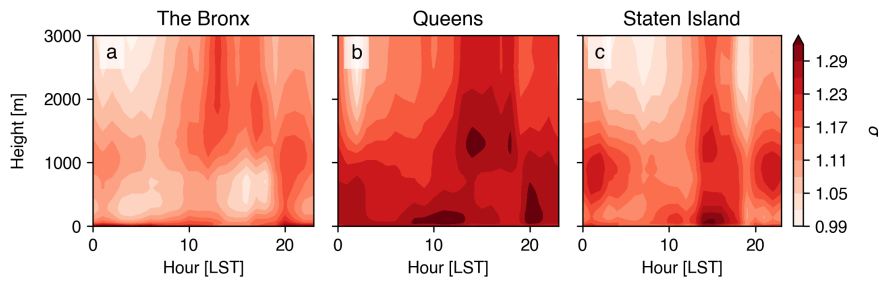


Figure 3: Anomalies of  $\theta$  during extreme heat events relative to the climatology over the urban boundary layer.

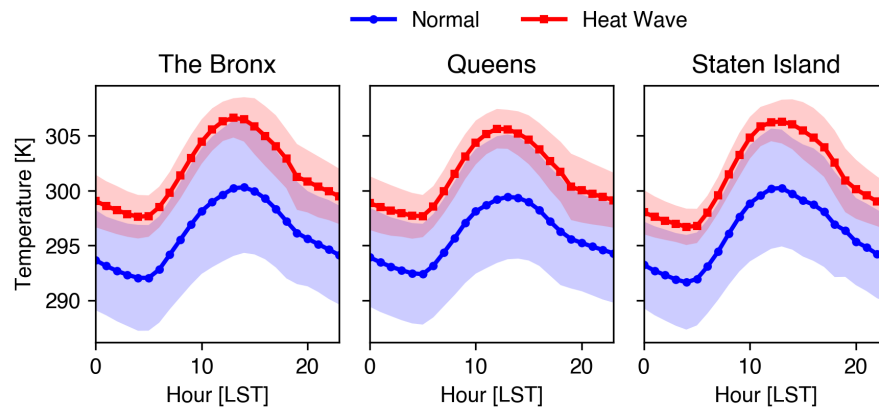


Figure 4: Anomalies of temperature during extreme heat events relative to the climatology at the surface.

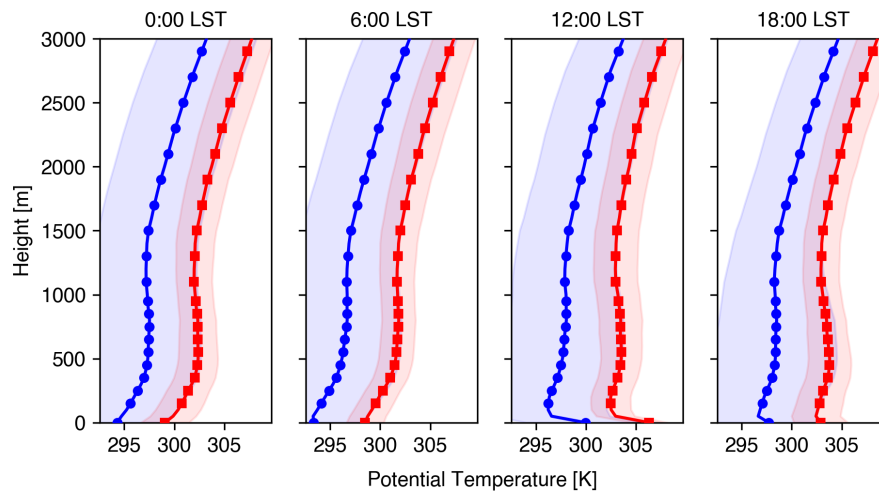


Figure 5: Vertical profiles of  $\theta$  in the Bronx during normal days (blue) and extreme heat events (red).

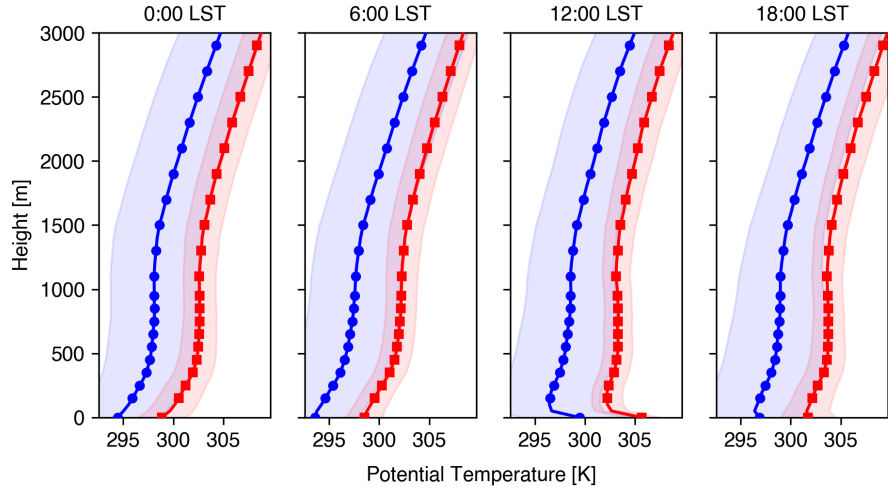


Figure 6: Vertical profiles of  $\theta$  in Queens during normal days (blue) and extreme heat events (red).

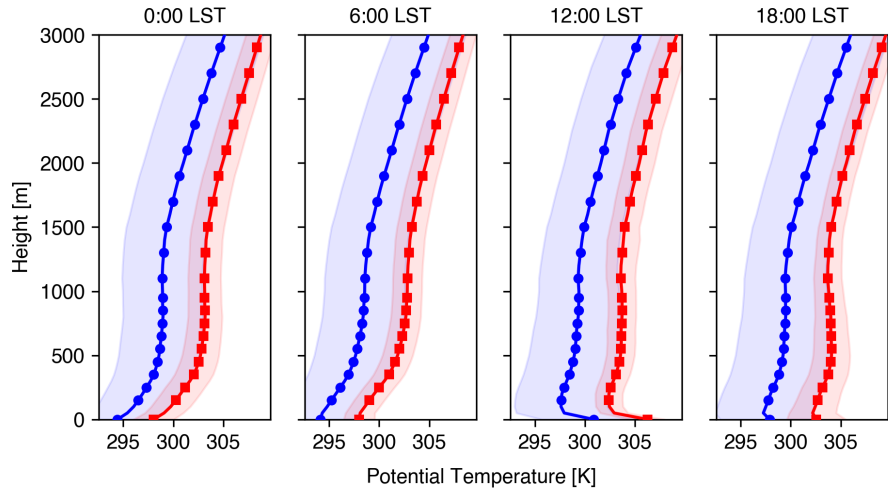


Figure 7: Vertical profiles of  $\theta$  in Staten Island during normal days (blue) and extreme heat events (red).

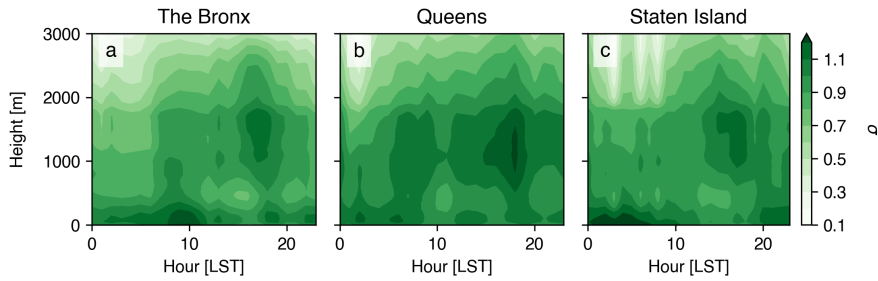


Figure 8: Anomalies of  $q$  during extreme heat events relative to the climatology over the urban boundary layer.

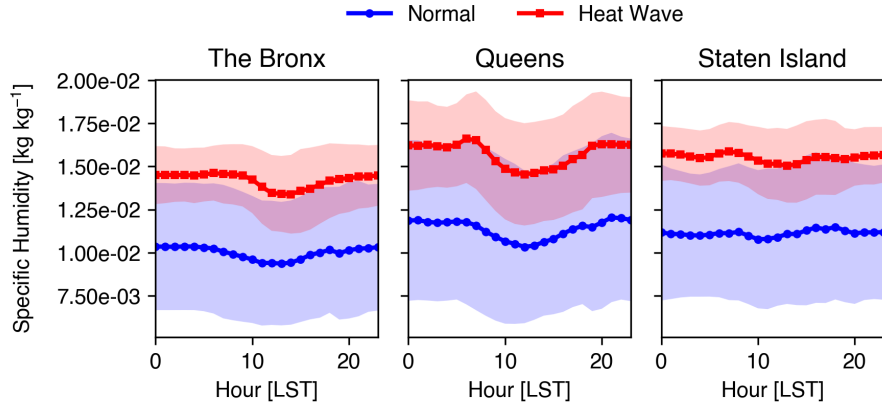


Figure 9: Anomalies of  $q$  during extreme heat events relative to the climatology at the surface.

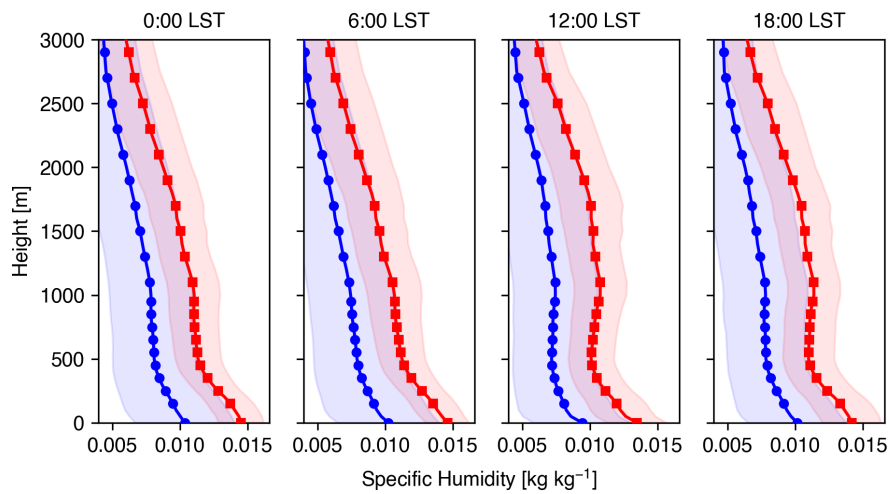


Figure 10: Vertical profiles of  $q$  in the Bronx during normal days (blue) and extreme heat events (red).

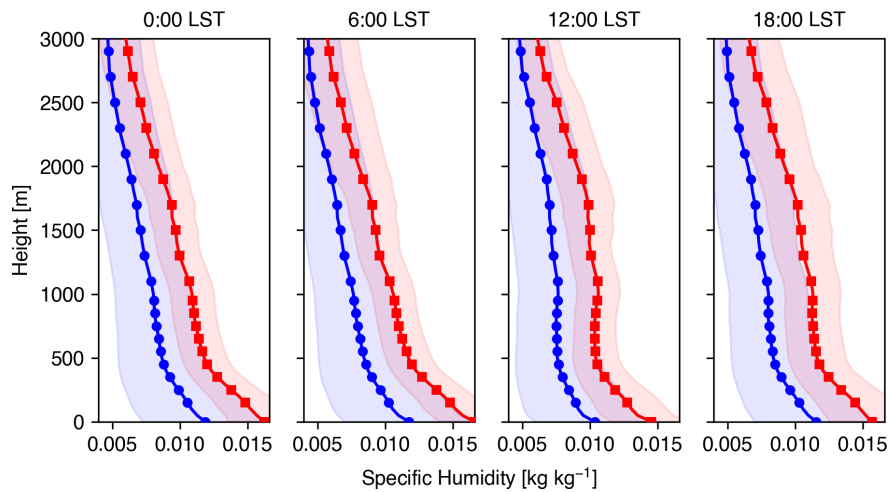


Figure 11: Vertical profiles of  $q$  in Queens during normal days (blue) and extreme heat events (red).

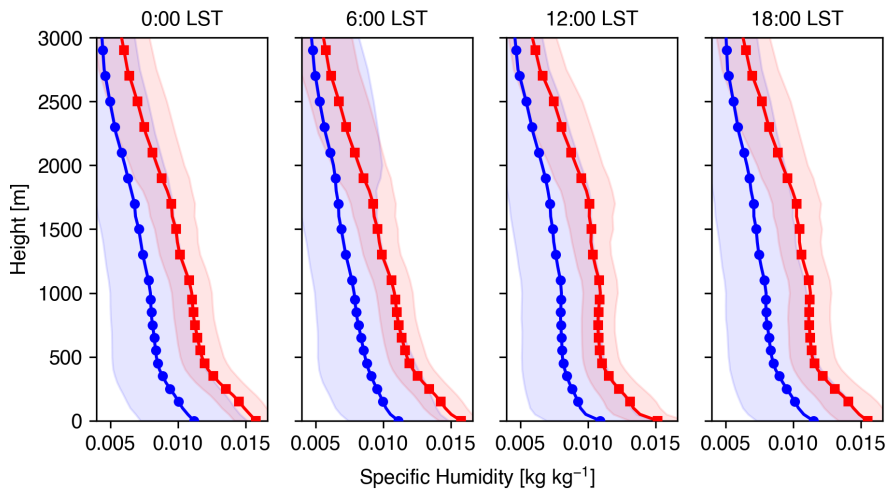


Figure 12: Vertical profiles of  $q$  in Staten Island during normal days (blue) and extreme heat events (red).

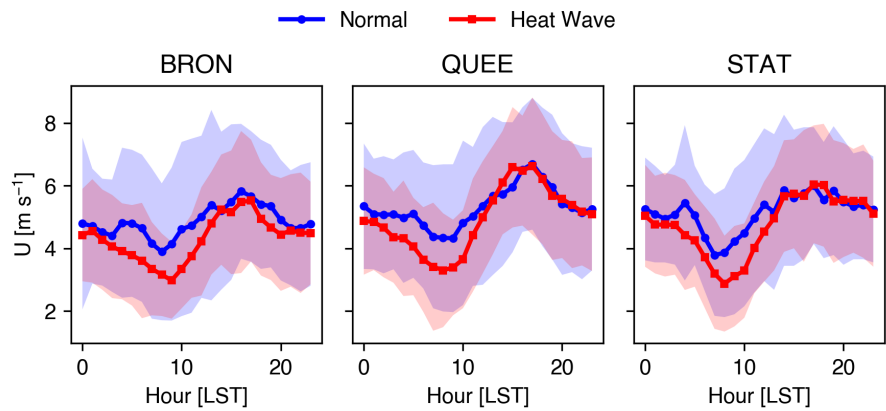


Figure 13: Anomalies of low-level  $U$  during extreme heat events relative to the climatology.

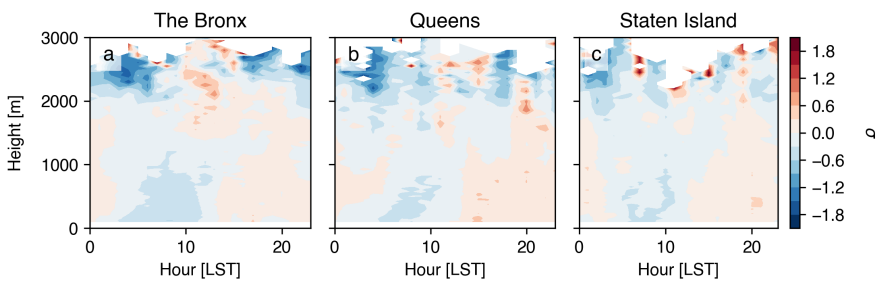


Figure 14: Anomalies of  $U$  during extreme heat events relative to the climatology over the urban boundary layer.

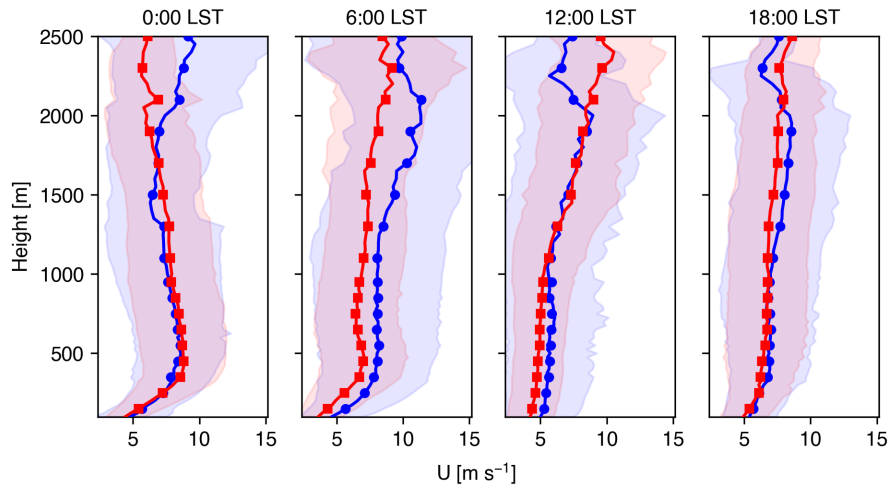


Figure 15: Vertical profiles of  $U$  in the Bronx during normal days (blue) and extreme heat events (red).

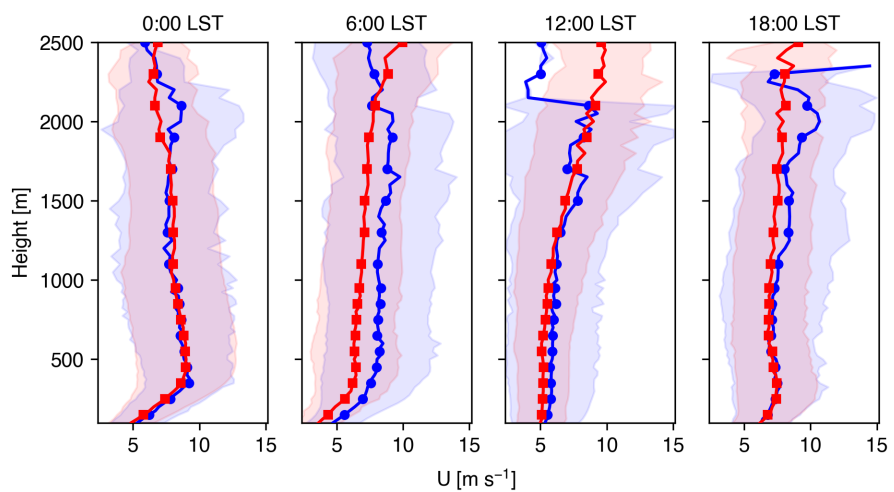


Figure 16: Vertical profiles of  $U$  in Queens during normal days (blue) and extreme heat events (red).

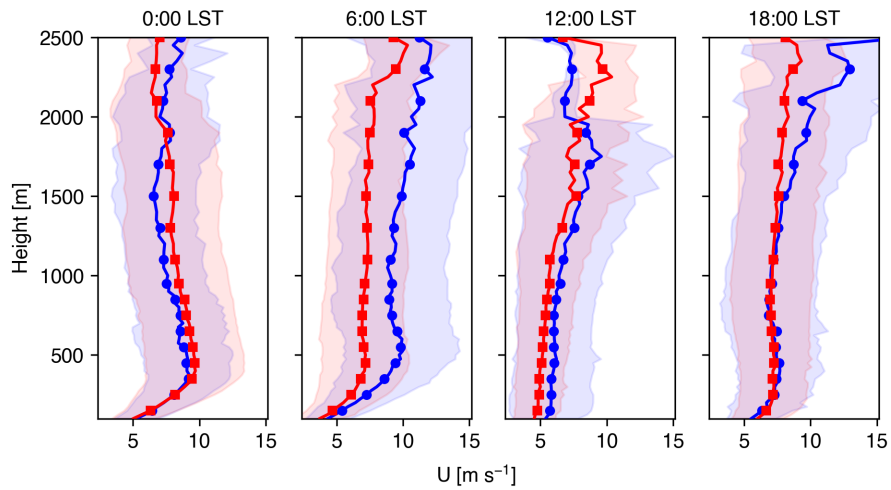


Figure 17: Vertical profiles of  $U$  in Staten Island during normal days (blue) and extreme heat events (red).

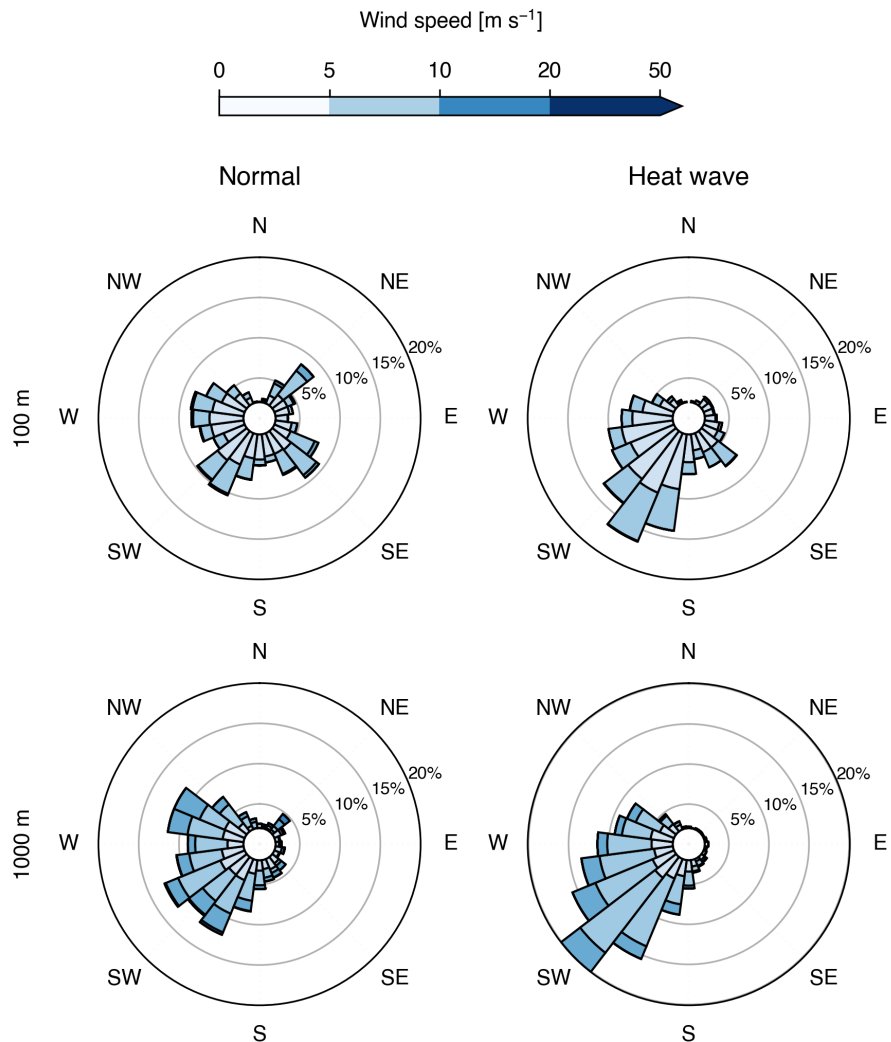


Figure 18: Horizontal winds in the lower-level (100 m) and mid-level of the urban boundary layer over the Bronx.

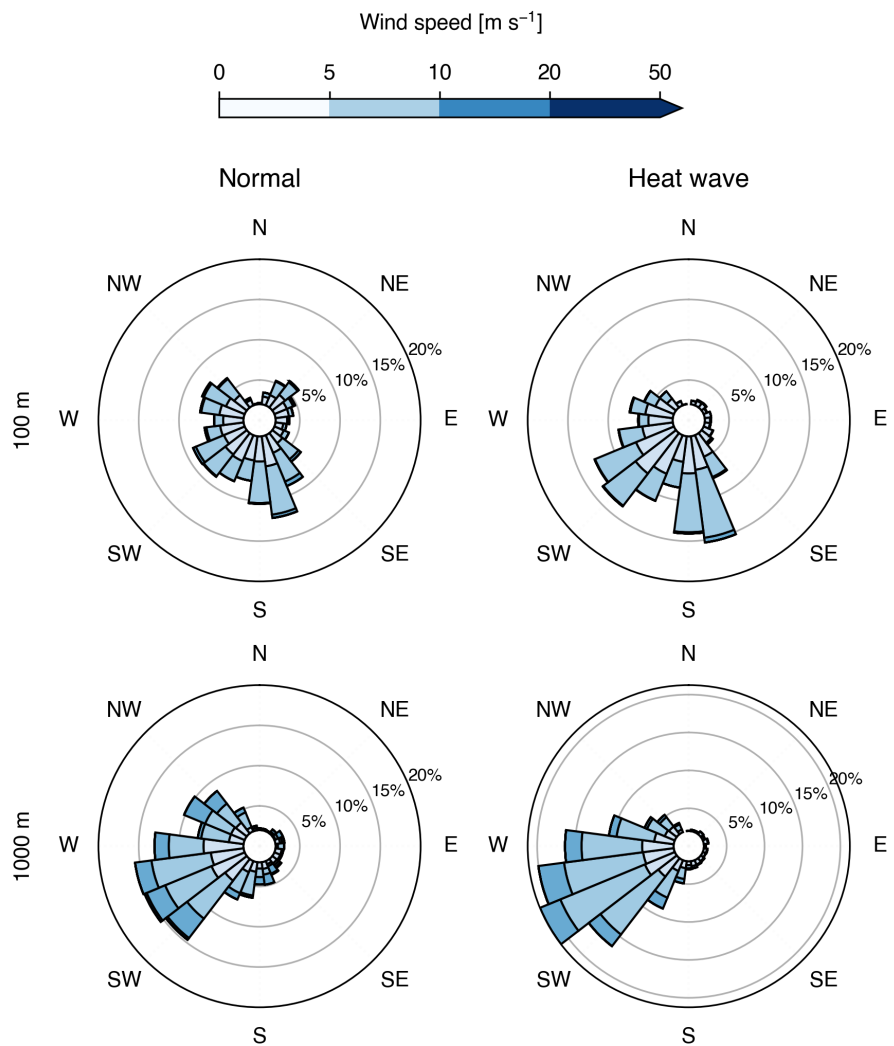


Figure 19: Horizontal winds in the lower-level (100 m) and mid-level of the urban boundary layer over Queens.

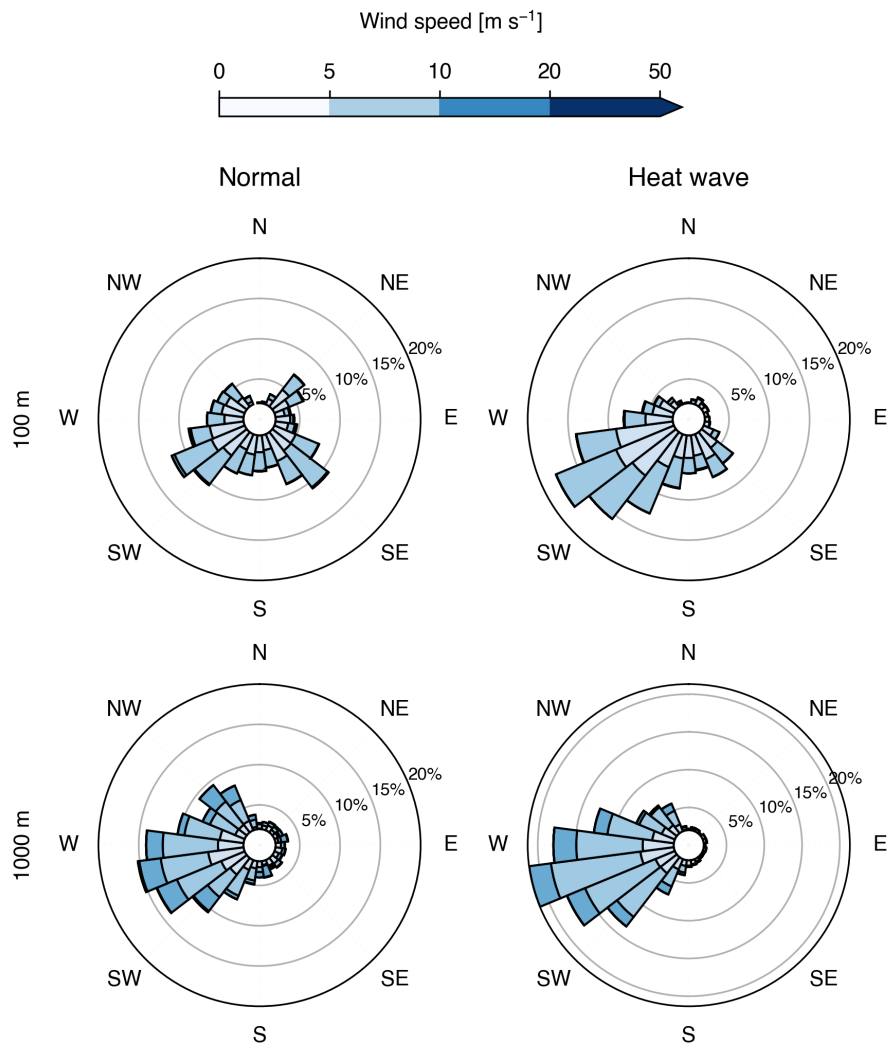


Figure 20: Horizontal winds in the lower-level (100 m) and mid-level of the urban boundary layer over Staten Island.

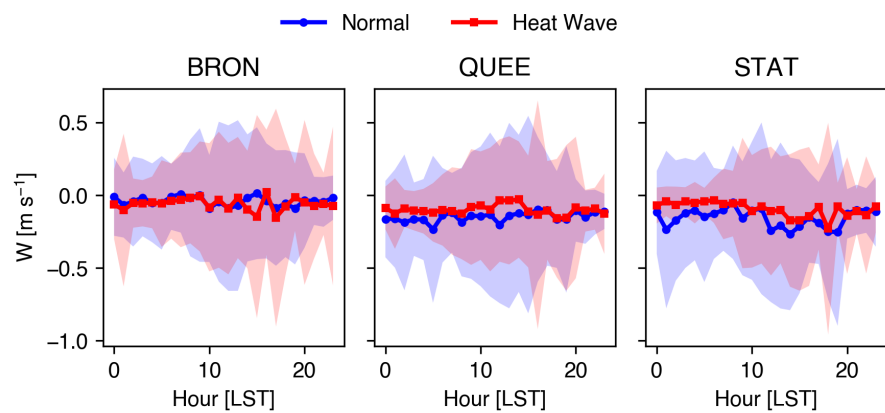


Figure 21: Anomalies of low-level  $w$  during extreme heat events relative to the climatology.

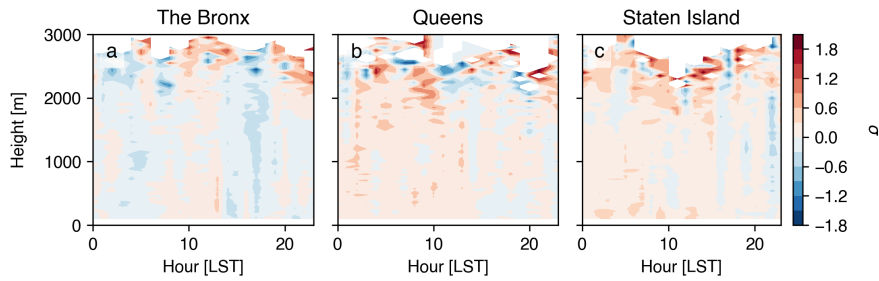


Figure 22: Anomalies of  $w$  during extreme heat events relative to the climatology over the urban boundary layer.

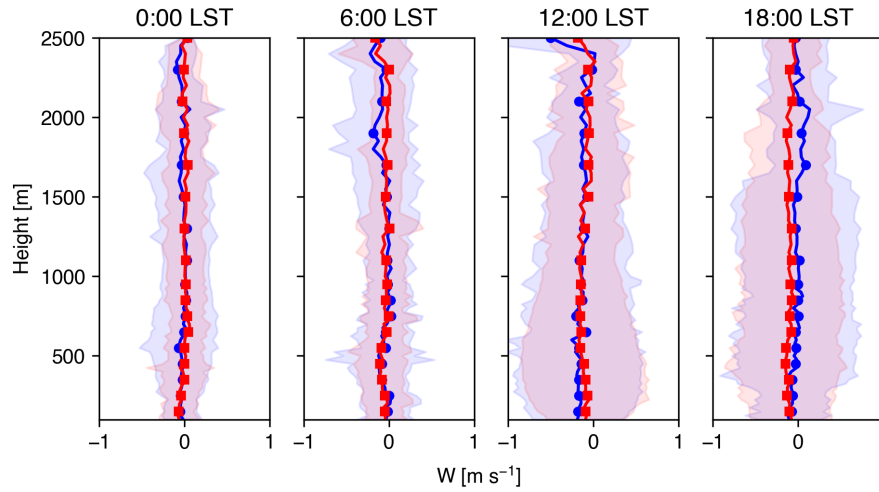


Figure 23: Vertical profiles of  $w$  in the Bronx during normal days (blue) and extreme heat events (red).

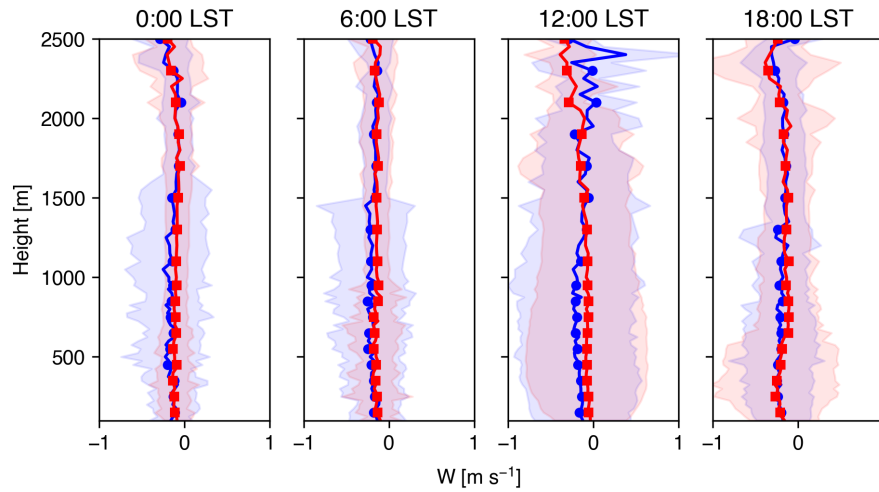


Figure 24: Vertical profiles of  $w$  in Queens during normal days (blue) and extreme heat events (red).

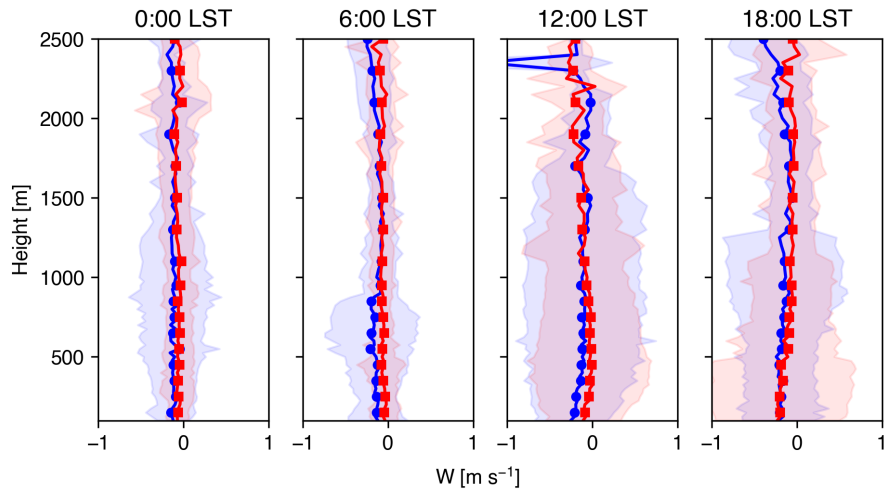


Figure 25: Vertical profiles of  $U$  in Staten Island during normal days (blue) and extreme heat events (red).

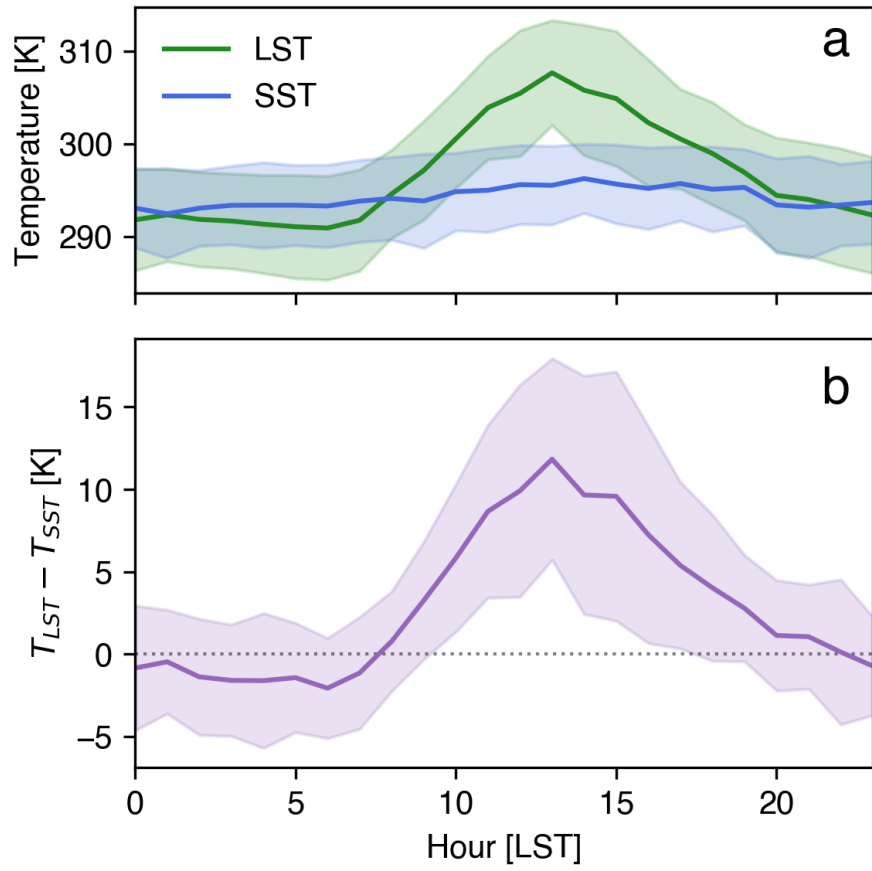


Figure 26: Temperature difference between Queens and New York Bight.

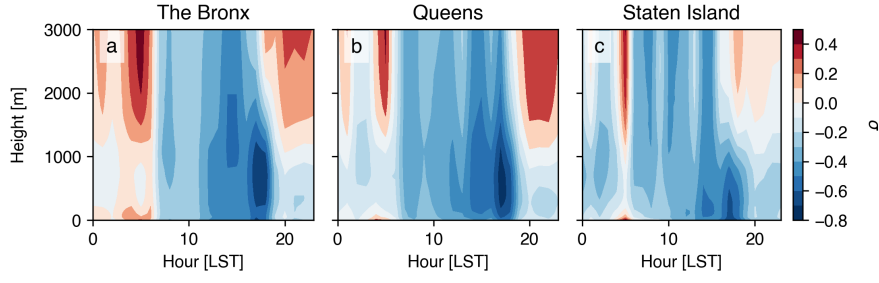


Figure 27: Anomalies of  $\theta$  for normal days with a sea breeze relative to normal days without a sea breeze.

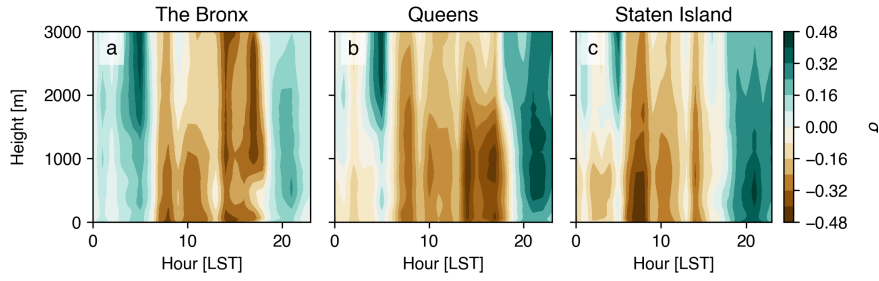


Figure 28: Anomalies of  $q$  for normal days with a sea breeze relative to normal days without a sea breeze.

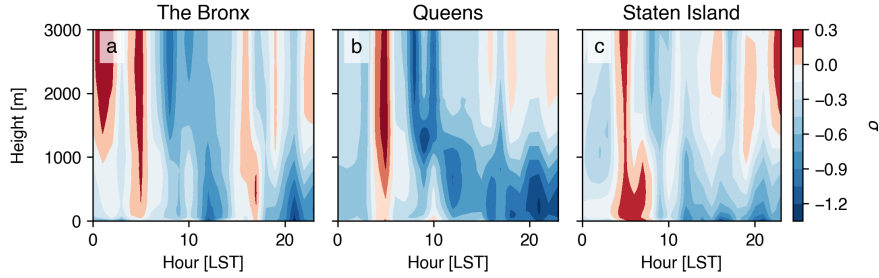


Figure 29: Anomalies of  $\theta$  for heat wave days with a sea breeze relative to heat wave days without a sea breeze.

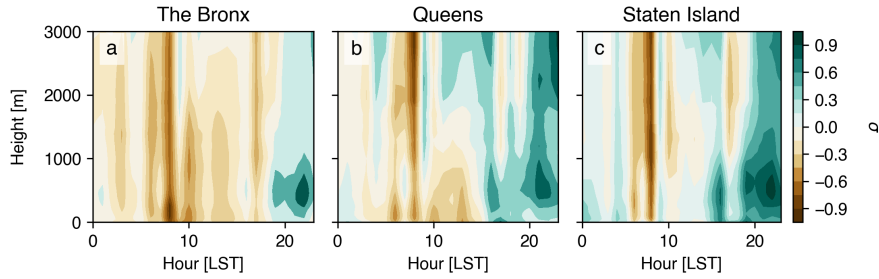


Figure 30: Anomalies of  $q$  for heat wave days with a sea breeze relative to heat wave days without a sea breeze.

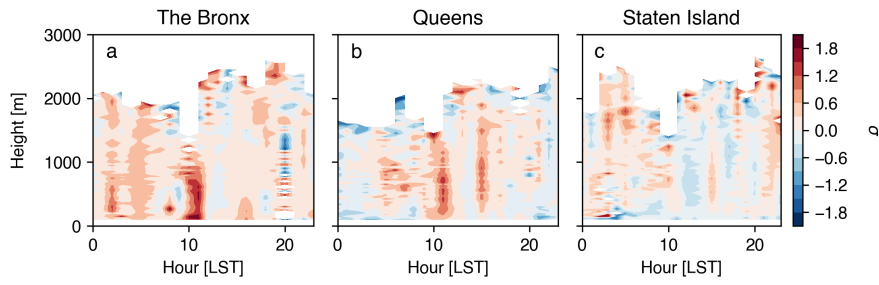


Figure 31: Anomalies of  $w$  for heat wave days with a sea breeze relative to heat wave days without a sea breeze.

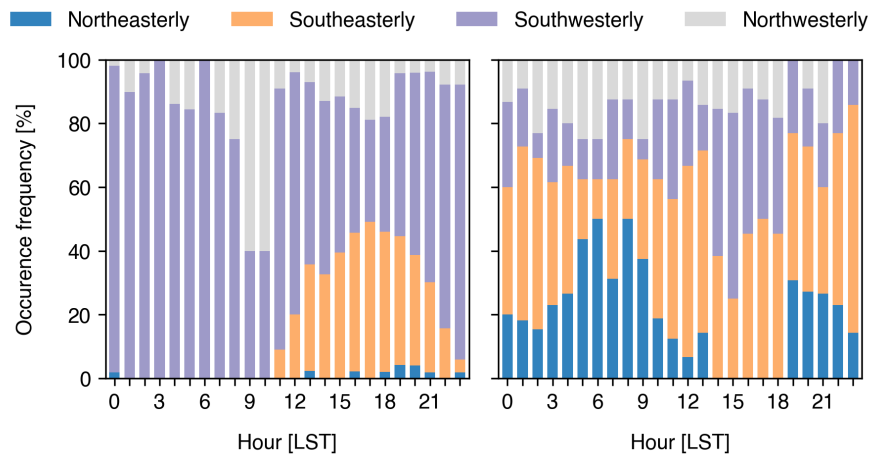


Figure 32: Occurrence frequency of wind directions at 100 m in the Bronx.

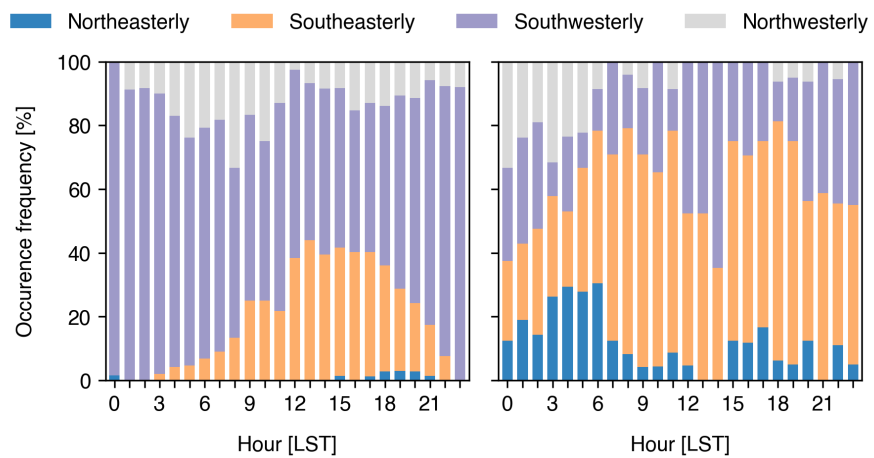


Figure 33: Occurrence frequency of wind directions at 100 m in Queens.

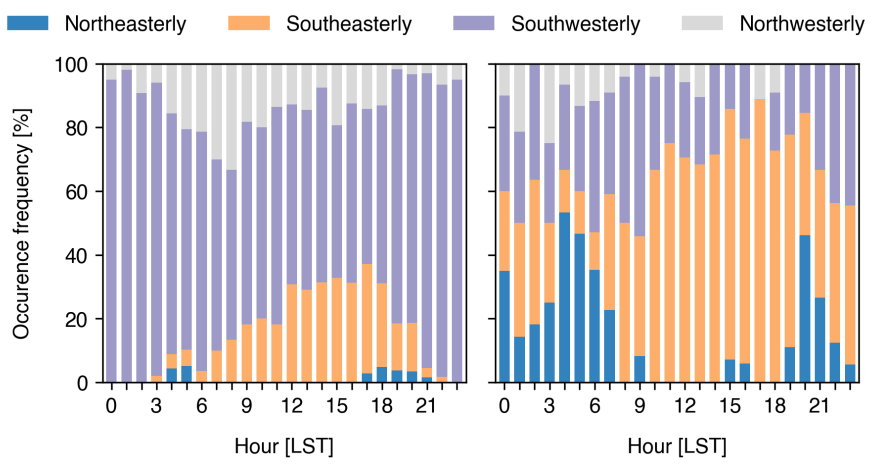


Figure 34: Occurrence frequency of wind directions at 100 m in Staten Island.